Applied Catalysis B: Environmental 180 (2016) 480–486

Contents lists available at ScienceDirect

Applied Catalysis B: Environmental

journal homepage: www.elsevier.com/locate/apcatb

Photocatalytic oxidation activities of TiO_2 nanorod arrays: A surface spectroscopic analysis

Yun Jeong Hwang[a], Sena Yang[b], Eun Hee Jeon[b], Hyun Woo Nho[c], Ki-Jeong Kim[d], Tae Hyun Yoon[c], Hangil Lee[e,*]

[a] Clean Energy Research Center, Korea Institute of Science and Technology, Seoul 136-791, Republic of Korea
[b] Molecular-Level Interface Research Center, Department of Chemistry, KAIST, 305-701, Republic of Korea
[c] Department of Chemistry, Hanyang University, 222 Wangsimniro, Seoul 133-791, Republic of Korea
[d] Beamline Research Division, Pohang Accelerator Laboratory (PAL), Pohang 790-784, Republic of Korea
[e] Department of Chemistry, Sookmyung Women's University, Seoul 140-742, Republic of Korea

ARTICLE INFO

Article history:
Received 27 April 2015
Received in revised form 3 July 2015
Accepted 6 July 2015
Available online 7 July 2015

Keywords:
Photo-oxidation reaction
TiO2 nanorods
Photocatalyst
HRPES
STXM

ABSTRACT

The correlation between the defect structures of hydrothermally grown TiO_2 nanorods (TNR) and their photocatalytic activity has been investigated by using various surface spectroscopic analysis techniques including scanning transmission X-ray microscopy (STXM) and high-resolution photoemission spectroscopy (HRPES). Defect states related to Ti^{3+} and oxygen vacancies in TNR were observed when the growth time was over 90 min (i.e., those over 500 nm in height), and these TNR samples showed photocatalytic oxidation activity with respect to the molecules 2-mercaptoethanol (2-ME) or 2-aminothiophenol (2-ATP), also confirmed by HRPES. The presence of defect structures on the TNR influences on the electronic states of titanium and oxygen, and thus can improve the catalytic oxidation reactions.

1. Introduction

For several decades, the chemical activities of the versatile formations of TiO_2 (thin films, nanoparticles, and nanorods) have been intensively studied because of the importance of this material in a variety of technologies, such as solar cells, photocatalysis, heterogeneous catalysis, gas sensing, medical implantation, and corrosion protection [1–5]. Especially, aligned TiO_2 nanostructures directly grown on a conducting substrate are favorable to electrical applications such photoelectrochemical water splitting, photoanodes of dye-sensitized solar cells, and optoelectronic applications [6]. To improve performances of the TiO_2 nanostructures, the previous studies have demonstrated the importance of controlling morphology, doping, surface treatment, and heterojunction formation with other materials [7–9]. To assist the further development, understanding the material properties is important, and surface spectroscopic analysis is a useful technique to characterize the chemical states which influence on their catalytic activities [10].

TiO_2 is a promising photocatalytic material, and many researchers have attempted to enhance the activities with nanostructures of TiO_2 nanoparticles (NPs) and nanorods (NRs) by using various fabrication methods. TiO_2 NRs (TNRs) can also enhance the oxidation reactions of various molecules, for example, from alcohol to aldehyde or carboxylic acid; from thiol to disulfide; from aniline to azobenzene, and so on [11–15]. TNR arrays can be easily synthesized on the substrate by a facile one-step hydrothermal reaction under the highly acidic condition [16–17] in which TiO_2 can be crystallized and etched during the reaction to have a one-dimensional (1D) growth. Their morphology changes over the growth time were well characterized by a scanning electron microscopy (SEM) and a transmission electron microscopy (TEM), and it has been assumed that the difference on the activity was mostly originated from the morphological changes. However, their electronic states related to defect structures, which have been relatively less characterized, are also important to determine the catalytic performance.

In this study, the hydrothermally synthesized TNRs were structurally characterized by using various surface techniques including SEM, X-ray diffraction (XRD), scanning transmission X-ray microscopy (STXM), and high-resolution photoemission spectroscopy (HRPES). We also focus on the photocatalytic activity of TNR arrays in the oxidation reactions of 2-ME (Scheme 1a) and

* Corresponding author. Fax: +82 2 2077 7321.
E-mail address: easyscan@sookmyung.ac.kr (H. Lee).

http://dx.doi.org/10.1016/j.apcatb.2015.07.004
0926-3373/

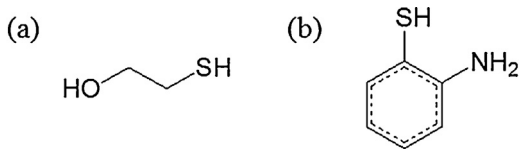

Scheme 1. The structures of (a) 2-mercaptoethanol (2-ME) and (b) 2-aminothiophenol (2-ATP).

2-ATP (Scheme 1b). With this approach, we evaluated the defects of TNRs and their photocatalytic oxidation activity.

2. Experimental

2.1. Preparation of TiO_2 nanorod samples

Three different TNR array samples were directly grown on fluorine-doped tin oxide (FTO) substrates varying the growth time. Each FTO substrate was cleaned through sonication in a 1:1:1 (volume ratio) mixture of deionized (DI) water, acetone, and isopropanol for 30 min, then rinsed with DI water and dried with nitrogen gas. 30 mL of concentrated HCl (Aldrich, 37.5%) was diluted with 30 mL of DI water, and 1 mL of titanium isopropoxide (Aldrich, 97.0%) was added slowly. The mixed solution was stirred for 2 h before transfer to a Teflon-lined autoclave. The conductive side of the FTO substrate was placed face down in the precursor solution, and the autoclave was placed in an oven at 200 °C for 60–150 min. After each reaction (the reaction times were 60, 90, and 150 min, resulting in TiO_2 nanorod samples denoted TNR-60, TNR-90, and TNR-150, respectively), the autoclave was cooled slowly outside of the oven, and the TiO_2 sample was rinsed with DI water. Finally, each sample of hydrothermally grown TiO_2 was annealed in air at 400 °C for 1 h

2.2. Photocatalytic oxidation reactions

2-Mercaptoethanol ($HOCH_2CH_2SH$, Sigma–Aldrich, 99% purity) and 2-aminothiophenol ($C_4H_4SHNH_2$, Sigma–Aldrich, 99% purity) were purified by turbo pumping prior to dosing onto the three TNR samples. A direct dozer controlled by means of a variable leak valve was used to dose the molecules onto the TNR arrays. The TNR samples were irradiated with UV light (λ = 365 nm, VL-4.LC. Tube 1 × 4-W, Vilber Lourmat) through a quartz window of a vacuum chamber. The pressure of the chamber was maintained at 10^{-6} Torr during dosing, and the number of exposed molecules was defined by the dosing time in seconds: 1 L (Langmuir) corresponds to 1 s dosing under 10^{-6} Torr.

2.3. Material characterizations

HRPES experiments were performed at the 8A2 beamline at the Pohang Accelerator Laboratory (PAL), which was equipped with an electron analyzer (R2000, Gamma data Scienta). The Ti 2*p*, O 1*s*, and S 2*p* core-level spectra were obtained by using photon energies of 510, 590, and 230 eV, respectively, to enhance the surface sensitivity. The binding energies of the core-level spectra were determined with respect to the binding energies of the clean Au 4*f* core-level for the same photon energy. All spectra were recorded in the normal emission mode. The photoemission spectra were carefully analyzed by using a standard nonlinear least-squares fitting procedure with Voigt functions [18]. STXM images and X-ray absorption near edge spectra were obtained at the SM beamline of the Canadian Light Source (CLS) with the monochromatic soft X-rays generated by the 2.9 GeV synchrotron source and a 250 mA storage ring [19]. The Fresnel zone plate (ZP) with an outermost zone width of 25 nm was used to focus the X-rays onto the TNR on the TEM grids. An order sorting aperture was installed between the ZP and the sample to collect the first order light diffracted by the ZP. The transmitted intensity was measured with a scintillation-photomultiplier tube (PMT). Image stacks were acquired at 445–485 eV and 520–570 eV with X-ray absorption spectroscopy (XAS) to extract the Ti *L*-edge and O *K*-edge spectra, which were obtained with exit slits of 20/20 and 20/15 mm (dispersive/non-dispersive) respectively. The STXM data was analyzed by using aXis 2000 (open source software developed by the Hitchcock group, http://unicorn.mcmaster.ca/aXis2000.html). The Ti *L*-edge and O *K*-edge

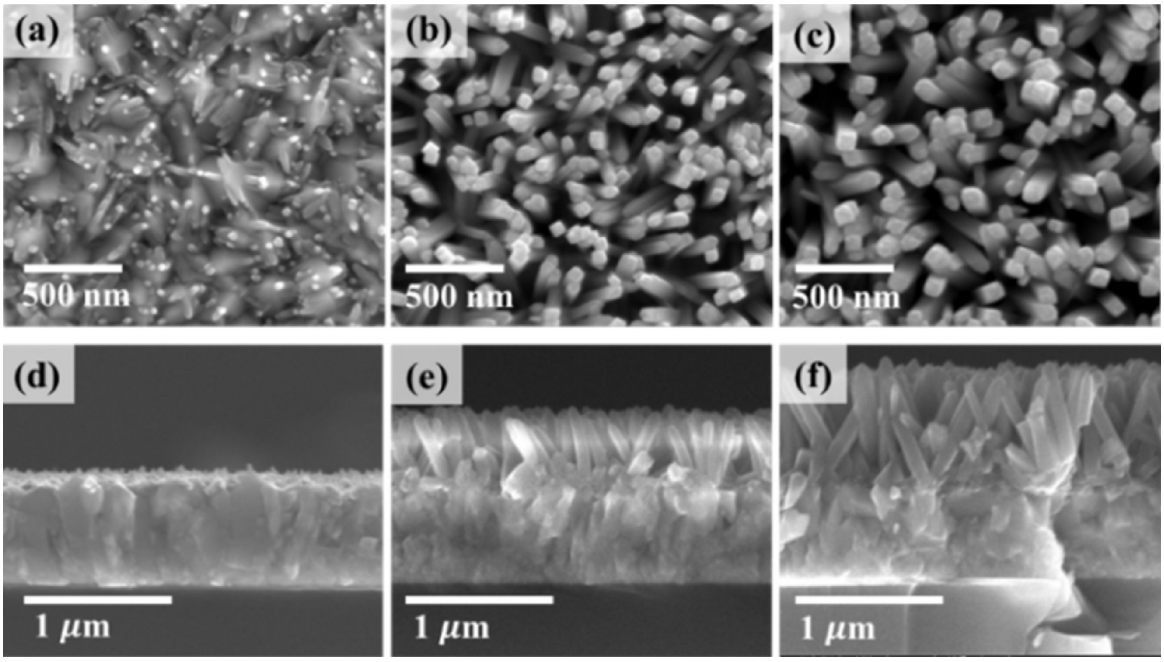

Fig. 1. Top-view and cross-sectional SEM images of TiO_2 nanorod (TNR) arrays grown on FTO substrates for 60 min (a) and (d): TNR-60, 90 min (b) and (e): TNR-90, and 150 min (c) and (f): TNR-150. The average heights of the TNRs are 50 nm, 500 nm, and 870 nm, respectively.

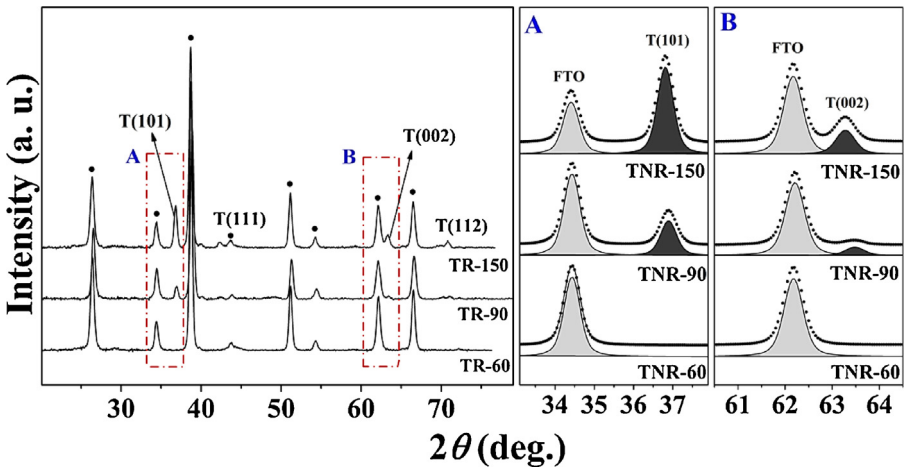

Fig. 2. Left panel: XRD data for TNR-60, TNR-90, and TNR-150. The solid dots indicate peaks due to the FTO substrate; the other peaks confirm the presence of rutile TiO_2. Middle panel: the magnifications of the peaks in the rectangular box A show the variation in the ratio of the intensities of the FTO and T(1 0 1) peaks. Right panel: the magnifications of the peaks in rectangular box B show the variation in the ratio of the intensities of the FTO and T(0 0 2) peaks.

spectra of the nanorods were collected from selected regions of interest in the image stacks to minimize the XAS contributions from the support films on the TEM grids. SEM images of the samples were obtained by using a field-emission scanning electron microscope (FEI, Inspect F50) operated at an acceleration voltage of 15 kV. XRD 2θ scans of the TNR arrays were acquired with a Bruker D8 Discover GADDS diffractometer by using Cu $K\alpha$ radiation.

3. Results and discussion

The evolution of 1D TiO_2 nanostructures was observed by examining SEM images of the samples (Fig. 1). Fig. 1a and d show that TNR-60 contained short and a particle-like irregular TiO_2 nanostructures attached to the FTO substrate, while 1D geometries were obtained as the growth time increased to 90 and 150 min. TNR-90 and TNR-150 appeared to have rectangular shapes and well-faceted side walls. These SEM images show that the structural morphology of TNR-60 is different from those of other two samples.

Next, we characterized the crystal structure of prepared TNRs by using XRD measurements (Fig. 2). Due to the small amount of TiO_2 (Fig. 1a and d), only FTO substrate peaks are evident for TNR-60, but the results for the other two samples clearly show that the hydrothermally grown TNRs on the FTO substrates have a rutile crystal structure. In addition, we also confirmed that TNR-

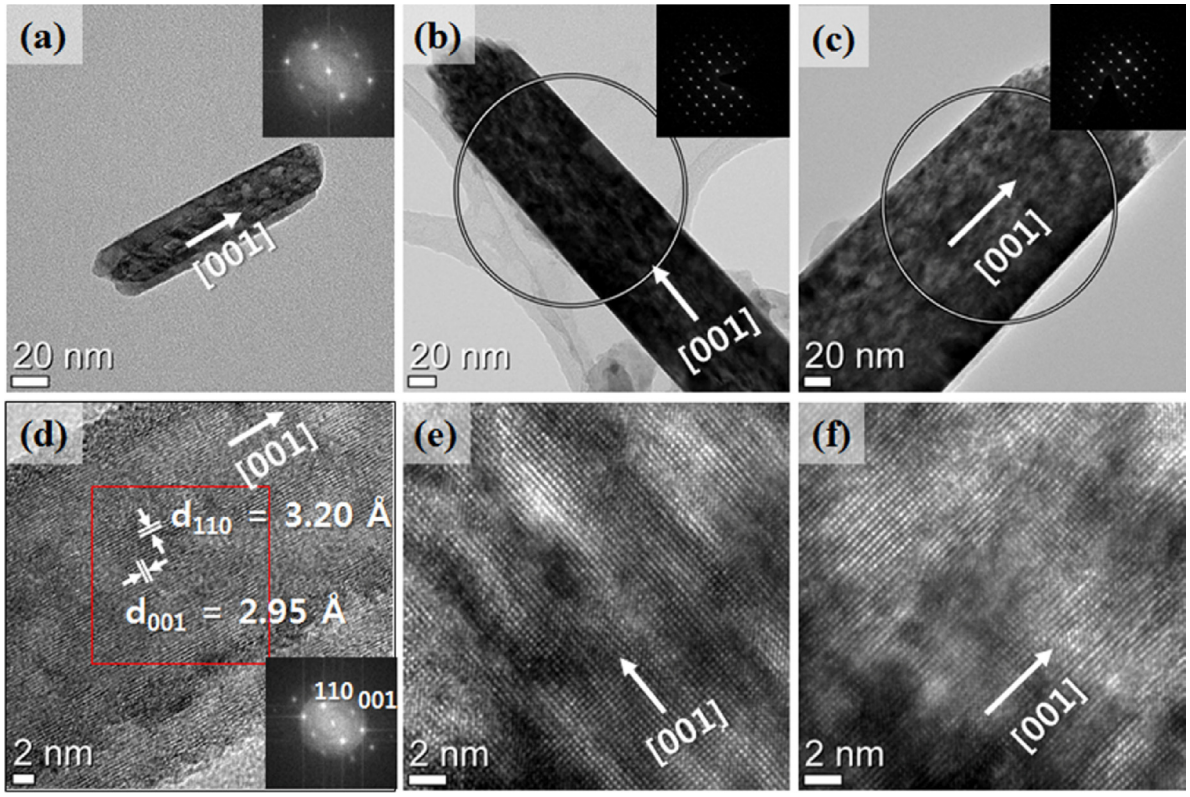

Fig. 3. TEM images of TiO_2 nanorod (TNR) arrays grown on FTO substrates for (a) 60 min (TNR-60), (b) 90 min (TNR-90), and (c) 150 min (TNR-150), and (d)–(f) magnified images of (a)–(c), respectively. The insets show the diffraction patterns.

60 consists of the same rutile phase by examining high-resolution transmission electron microscopy (HRTEM) images (Fig. 3a and d).

Fig. 3 shows that the measured lattice fringes in the HRTEM images is matched with d spacing of d_{110} = 3.20 Å and d_{001} = 2.95 Å, which are characteristic of rutile phase TiO_2. The growth direction of the NR is [0 0 1] with side walls of [1 1 0] facets in all three samples, which is consistent with previous reports [16]. To clarify the correlation between growth time and the facets of the TNR arrays, we examined the two facet-induced peaks that arise at $2\theta = 36.5^\circ$ and 63.0°, which are associated with the {1 0 1} and {0 0 2} planes, respectively [20]. The intensities of these peaks in the spectra of TNR-90 and TNR-150 were compared. The relative intensities of I_{101}/I_{002} were 8.2 and 5.3 for TNR-90 and TNR-150 respectively, which indicates that the peak intensity for {0 0 2} increases rapidly as the growth duration increases. This result is associated with the [0 0 1] growth direction of the TNR [21]. The structural analyses clearly confirm that the growth time of TiO_2 is closely related to its morphology and facets [22].

For the more detail characterization, STXM images and the corresponding XAS spectra for TNR-60 and TNR-150 were investigated to compare their Ti and O electronic states (Fig. 4) which showed significant discrepancy between TNR-60 and TNR-150. The black regions in Fig. 4a–d originate from TNRs as we obtained at the fixed energies of Ti *L*-edge and O *K*-edge regions. The Ti *L*-edge spectra as shown in Fig. 4e and g (TNR-60 and TNR-150 respectively) indicate the presence of typical rutile TiO_2 structure according to the ratio of the d_z^2 and $d_{x^2-y^2}$ intensities of the e_g orbital located at ~460 eV [23–25]. Although we have confirmed that both TNR-60 and TNR-150 contain rutile TiO_2 nanostructures, there are also crucial differences between them. In particular, the ratios of the intensities of the t_{2g} and e_g orbitals are different, which indicates slight differences in their exposed surface facets and defect structures. Moreover, the intensities of the two pre-edge peaks of TNR-150 (left bottom panel: marked C) located at 456.7 and 457.4 eV are larger than those of TNR-60 (left bottom panel: marked A), which indicates that these peaks are induced by surface defect structures (the Ti^{3+} state) [26,27]. The XAS analysis showed that the number of defect structures increases as the growth time increases.

Moreover, another difference was observed from the O *K*-edge XAS spectra of the TNR-60 and TNR-150 samples (Fig. 4f and h). There are large differences between the intensities of the two pre-peaks at 530–540 eV (right bottom panel: marked B and D). It is well known that the low-energy range of the spectrum (530–540 eV) is due to transitions from the O 1*s* core-level orbital to the O 2*p* orbital [23,24,28], which implies the different electronic structures in TNR-60 and TNR-150. Defect structures can influence on the interactions between the O 2*p* and Ti 3*d* orbitals causing the variation of O *K*-edge XAS spectra despite the same rutile crystal structures.

HRPES measurement was also performed to characterize the oxidation states of Ti and O elements in the three different TNR samples. The core-level spectra (Ti 2*p* and O 1*s*) of the bare TNRs

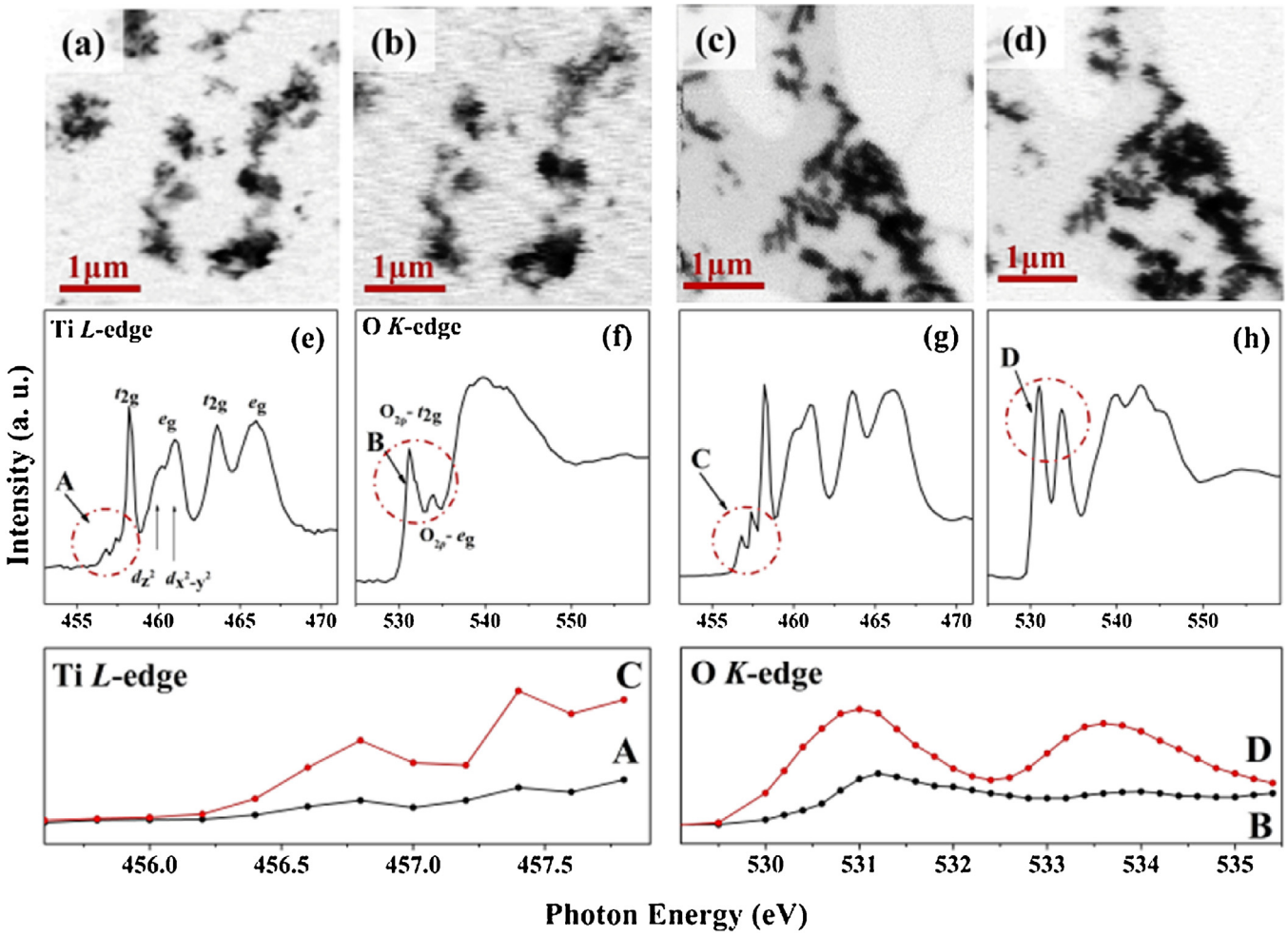

Fig. 4. STXM images (4 μm × 4 μm) of the TiO_2 nanorods (TNR) and their corresponding XAS spectra. STXM images for TNR-60 (a) 459.0 eV and (b) 530 eV, and for TNR-150 (c) 459.0 eV and (d) 530 eV. XAS spectra for TNR-60: (e) Ti *L*-edge and (f) O *K*-edge, and for TNR-150: (g) Ti *L*-edge and (h) O *K*-edge.

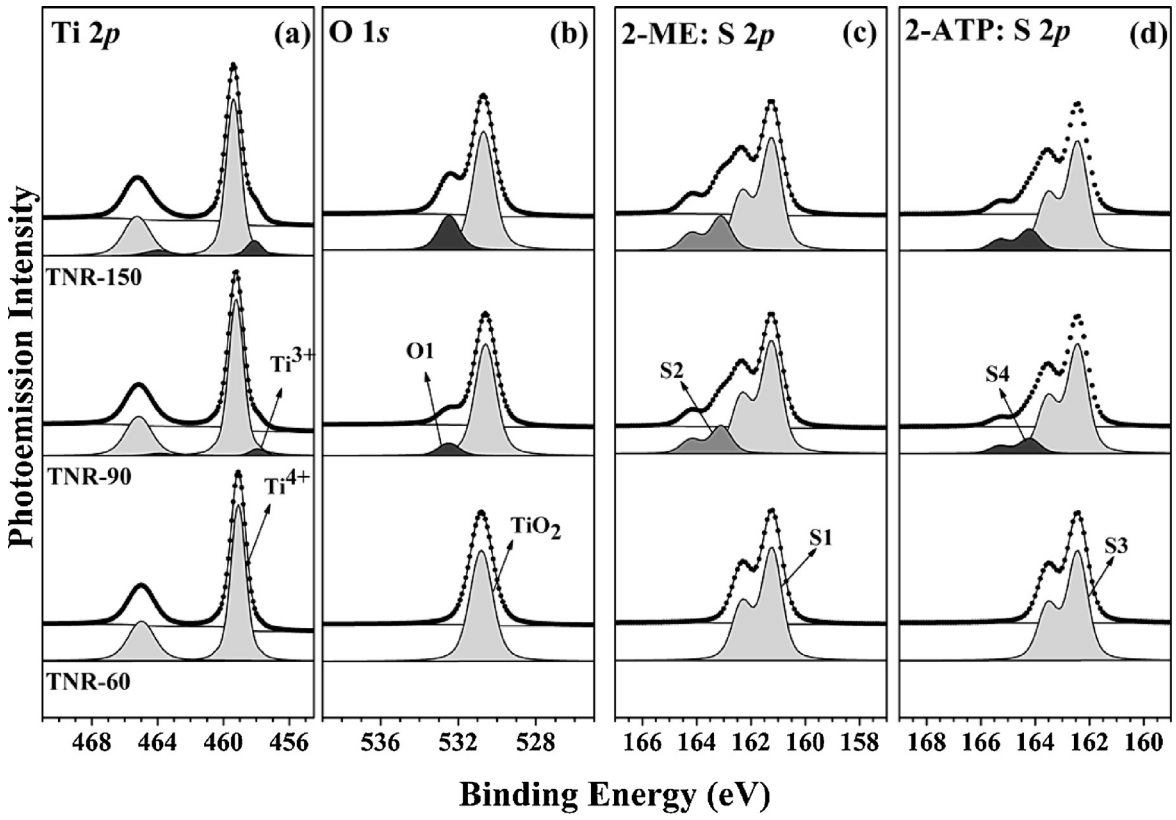

Fig. 5. HRPES core-level spectra for TiO_2 nanorods (TNR-60, TNR-90, and TNR-150): (a) Ti 2*p* and (b) O 1*s*. HRPES S 2*p* core-level spectra for the three TNR samples with adsorbed (c) 2-ME (360 L) and (d) 2-ATP (360 L).

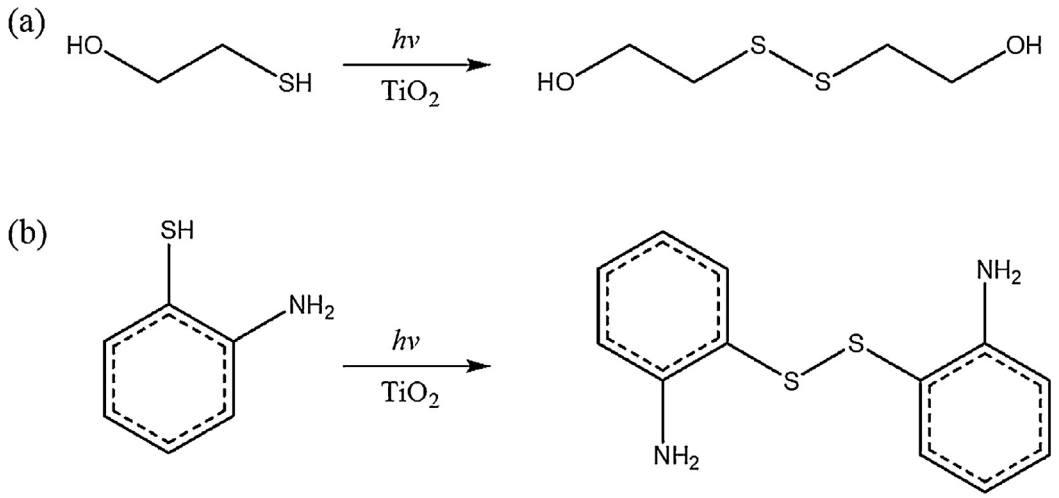

Fig. 6. Photocatalytic oxidation reactions of (a) 2-ME and (b) 2-ATP on TiO_2 nanorods.

(Fig. 5a and b) also showed distinct discrepancy between TNR-60 and TNR-90 (or TNR-150) which consistently suggested the presence of the defect states on TNR-90 (or TNR-150) samples. Ti 2*p* and O 1*s* core-level peaks of TNR-60 contain only independent single features, respectively, without any minor peaks, and their binding energies were found to be 459.3 and 530.7 eV, which are well matched with the binding energies of crystalline TiO_2. In general, bulk TiO_2 particles have the each binding energy at 459.3 ± 0.1 and 530.6 ± 0.1 eV [29–31]. When the growth time increased to 90 min and beyond (TNR-90 and TNR-150), additional binding peaks were observed both in the Ti 2*p* and O 1*s* core-level spectra. These spectra contain two distinctive features: Ti 2*p* at 459.3 eV (Ti^{4+}) and 458.0 eV (Ti^{3+}) [32,33], O 1*s* at 530.6 eV (TiO_2) and 532.8 eV (defect related O 1*s*), and TNR-150 had a larger ratio of additional peaks. The evolution of minor peaks clearly indicates the partial formation of Ti^{3+} defect structures on the hydrothermally grown TNR as the growth time increased. Both XAS and HRPES result revealed the differences of the Ti and O electronic states between TNR-60 and TNR-150, related to oxygen vacancy defects, meaning the defect states in TNR increased as the growth time increased.

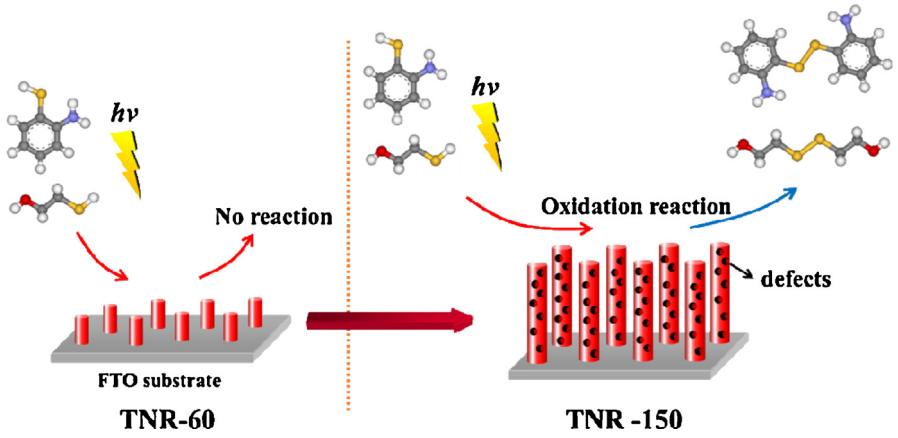

Scheme 2. Enhanced photocatalytic oxidation of 2-ME and 2-ATP on TiO_2 nanorod arrays (TNR-150) containing the surface defect states.

Next, we investigated and compared the photocatalytic activities of the three TNR samples, which showed distinguishable result between TNR-60 and TNR-90 (or TNR-150). For the photocatalytic reaction, 2-mercaptoethanol (2-ME) or 2-aminothiophenol (2-ATP) molecules were exposed with the same amount of molecular oxygen under 365 nm UV light illumination onto the TNR samples. The oxidations of the molecules were monitored by observing the changes in the S 2*p* peaks in the HRPES measurement, which were obtained at a photon energy of 230 eV. Fig. 5c shows the surface-sensitive S 2*p* spectra after co-exposing 360 L (1L = 10 s times 1×10^{-7} Torr in our experimental condition) of 2-ME with the same amount of oxygen on the three TNR samples. In the case of 2-ME adsorbed on TNR-60, there was only a single S 2*p* peak located at 161.3 eV, a thiol-induced peak (unbounded), implying no photo-oxidation has occurred [34,35]. In contrast, the spectra of the other two TNR samples (TNR-90 and TNR-150) contain two distinct sulfur peaks corresponding to the thiol peak (at 161.3 eV, marked S1) and the disulfide peak (at 163.1 eV, marked S2), which are due to the oxidation of the thiol group. These changes in the sulfur peaks indicate that oxidation of 2-ME has occurred both on TNR-90 and TNR-150 [36].

Similarly, oxidation of thiol group attached on the aromatic ring (Fig. 5d) was monitored with 2-ATP molecules through the changes of S 2*p* core-level spectra, after deposition of 360 L 2-ATP. Again, TNR-60 had only a single feature at 162.4 eV (marked S3), indicating no oxidation of 2-ATP. Meanwhile, the spectra for the other two samples contain two distinct sulfur peaks corresponding to the thiol peak (at 162.4 eV, marked S3) and the disulfide peak of 2-ATP (at 164.2 eV, marked S4), which are due to the oxidation of the thiol group. The presence of disulfide peak indicated that photo-oxidation of 2-ATP occurred on TNR-90 and TNR-150 surface both of which had observable Ti^{3+} defect sites according to XAS and HRPES measurements. In addition, compared to TNR-90, TNR-150 showed higher ratio of the disulfide peak to unbounded sulfur peak on the TNR surfaces indicating higher photocatalytic activity on TNR-150 surface. The photocatalytic oxidation reactions of 2-ME and 2-ATP on TiO_2 nanorods are described in Fig. 6 and Scheme 2.

These surface spectroscopic results suggest that the defect state is important to enhance the photo-oxidation activity of TNRs. Photocatalytic oxidation occurs on a TiO_2 surface through a charge transfer of photo-generated holes to the adsorbed molecules via the valence band of TiO_2. We expect that the variation in the Ti and O electronic states induced by the defect formation can contribute to the enhanced photocatalytic activities with TNR-90 and TNR-150 samples. Meanwhile, defects on the TiO_2 surface can be a recombination center, which can decrease the life time of the photogenerated charges resulting in decrease of photocatalytic activity. However, oxygen vacancy in TiO_2 has been also considered as a catalytic active site, and our experiments showed the enhanced activity of thiol group oxidation with TNR-90 and TNR-150.

Moreover, the ratios of the oxidized sulfur peaks (S2/S1 ratio of the adsorbed 2-ME and S4/S3 ratio of the adsorbed 2-ATP) on the TNR samples were examined by varying the dosing amount of the

Fig. 7. The ratios of the intensities of (a) S2 and S1 and (b) S4 and S3 adsorbed on the three distinct TiO_2 NR samples as functions of molecular exposure under 365 nm UV light.

Table 1
The ratios of the intensities of S2 and S1 for 2-ME and of S4 and S3 for 2-ATP adsorbed on the three distinct TiO_2 nanorod samples as functions of exposure to 2-ME and 2-ATP under exposure to 356 nm UV light.

Exposure (L)	Intensity ratio under 356 nm UV light exposure					
	S2/S1			S4/S3		
Sample	TNR-60	TNR-90	TNR-150	TNR-60	TNR-90	TNR-150
15	0.00	0.07	0.14	0.00	0.04	0.06
30	0.00	0.12	0.17	0.00	0.07	0.10
100	0.00	0.16	0.21	0.00	0.11	0.15
200	0.00	0.21	0.27	0.00	0.14	0.19
360	0.05	0.25	0.31	0.00	0.16	0.20

reactant molecules (Fig. 7). Variations in the S2/S1 and S4/S3 intensity ratios are observed for all 2-ME and 2-ATP doses on TNR-90 and TNR-150, which showed more molecules were oxidized as the dosing amount increased. To be more specific, when the surface of TNR-150 is exposed to 360 L of 2-ME, the S2/S1 ratio is 0.31, which is 1.24 times higher than of the equivalent ratio for TNR-90 (0.25) (Table 1). The higher ratios of S2/S1 indicate that the oxidation of the adsorbed 2-ME molecules was more facilitated on TNR-150 compared to that on TNR-90. A similar trend was observed for the catalytic oxidation of 2-ATP on the TNRs. These photo-oxidation experimental results indicate that the photocatalytic activity of the hydrothermally grown TNR changed depending on the growth time, which has a positive correlation with the defect sites of the TNR.

4. Conclusions

Through surface spectroscopic measurements, we observed the evolution of defect structures related to the Ti^{3+} state or oxygen vacancies when crystalline TiO_2 nanorod arrays were hydrothermally grown on an FTO substrate above 500 nm in height (TNR-90 and TNR-150). Compared to TNR-60 and TNR-150 samples, XAS spectra showed changes of the electronic states in Ti L-edge and O K-edge, and HRPES also showed an addition peak at lower binding energy in the Ti 2*p* spectra and a peak at higher binding energy in the O 1*s* spectra, respectively, which are associated with the presence of the defect structures when the growth time increased. By performing the photo-oxidation reactions of two different molecules (2-ME and 2-ATP) on three distinct TiO_2 samples under UV illumination, we found that the photocatalytic –SH oxidation was facilitated with the NR samples which had the defect structures. Surface spectroscopic analysis was used to characterize the defect structures on the catalyst surfaces as well as photo-oxidation reaction; these techniques are applicable to investigations of the correlation between the defects and photo-oxidation activities of other semiconductor material systems.

Acknowledgement

This research was supported by the National Research Foundation of Korea (NRF) funded by the Korea government (MSIP) (No. 20090083525 and No. 2015021156).

References

[1] A. Fujishima, X. Zhang, D.A. Tryk, Surf. Sci. Rep. 63 (2008) 515–582.
[2] C.L. Pang, R. Lindsay, G. Thorntonb, Chem. Soc. Rev. 37 (2008) 2328–2353.
[3] Y. Du, N.A. Deskins, Z. Zhang, Z. Dohnálek, M. Dupuis, I. Lyubinetsky, Phys. Rev. Lett. 102 (2009) 0961021–0961024.
[4] Z. Zhang, O. Bondarchuk, J.M. White, B.D. Kay, Z. Dohnálek, J. Am. Chem. Soc. 128 (2006) 4198–4199.
[5] B. Liu, E.S. Aydil, J. Am. Chem. Soc. 131 (2009) 3985–3990.
[6] J.-J. Wu, C.-C. Yu, J. Phys. Chem. B. 108 (2004) 3377–3379.
[7] A. Zaleska, Recent Pat. Eng. 2 (2008) 157–164.
[8] M. Ni, M.K.H. Leung, D.Y.C. Leung, K. Sumathy, Renewable Sustainable Energy Rev. 11 (2007) 401–425.
[9] S.G. Kumar, L.G. Devi, J. Phys. Chem. A 115 (2011) 13211–13241.
[10] M.A. Aramendía, V. Borau, J.C. Colmenares, A. Marinas, J.M. Marinas, J.A. Navío, F.J. Urbano, Appl. Catal, B Environ. 80 (2008) 88–97.
[11] D.I. Enache, J.K. Edwards, P. Landon, B. Solsona-Espriu, A.F. Carley, A.A. Herzing, M. Watanabe, C.J. Kiely, D.W. Knight, G.J. Hutchings, Science 311 (2006) 362.
[12] M.J. Climent, A. Corma, S. Iborra, M. Mifsuda, Adv. Synth. Catal. 349 (2007) 1949–1954.
[13] Y. Shiraishi, S. Sugano, Angew. Chem. Int. Ed. 49 (2010) 1656–1660.
[14] C. Karunakaran, S. Senthilvelan, S. Karuthapandian, J. Photochem. Photobiol. A Chem. 172 (2005) 207–213.
[15] H. X. Lang, C. Ji, W. Chen, J. Zhao Ma, Angew. Chem. Int. Ed. 50 (2011) 3934–3937.
[16] B. Liu, E.S. Aydil, J. Am. Chem. Soc. 131 (2009) 3985–3990.
[17] Y.J. Hwang, C.H. Hahn, B. Liu, P. Yang, ACS Nano 6 (2012) 5060–5069.
[18] F. Schreier, J. Quant. Spectrosc. Radiat. Transfer 48 (1992) 743.
[19] H. Nho, J. Kim, J. Wang, H.-J. Shin, S.-Y. Choi, T. Yoon, J. Synchrotron Rad. 21 (2014) 170–176.
[20] K. Thamaphat, P. Limsuwan, B. Ngotawornchai, J. Kasetsart, J. Nat. Sci. 42 (2008) 357–361.
[21] X. Bai, B. Xie, N. Pan, X. Wang, H. Wang, J. Solid State Chem. 181 (2008) 450.
[22] W. Zhang, J. Fu, H. Xi, S. He, H. Zhao, J. Alloys Compd. 575 (2013) 40–47.
[23] Y. Hwu, Y.D. Yao, N.F. Cheng, C.Y. Tung, H.M. Lin, NanoStruct. Mater. 9 (1997) 355–358.
[24] L.D. Finkelstein, E.I. Zabolotzky, M.A. Korotin, S.N. Shamin, S.M. Butorin, E.Z. Kurmaev, J. Nordgren, X-ray Spectrosc. 31 (2002) 414–418.
[25] P. Krüger, Phys. Rev. B 81 (2010) 125121.
[26] S. M. Kareev, J. Prosandeev, C. Liu, A. Gan, J. W. Freeland Kareev, J. Chakhalian Min Xiao, Appl. Phys. Lett. 93 (61) (2008) 909.
[27] Y. S. B. Singh, Y. Wang, H. Shao, S. Lai, M. V. Limaye Hsieh, C. Chuang, H. Hsueh, H. Wang, J. Chiou, H. Tsai, C. Pao, C. Chen, H. Lin, J. Lee, C. Wu, J. Wu, W. Pong, T. Ohigashi, N. Kosugi, J. Wang, J. Zhou, T. Regier, Nanoscale 6 (2014) 9166–9176.
[28] F.M.F. de Groot, J. Faber, J.J.M. Michiels, M.T. Czyżyk, M. Abbate, J.C. Fuggle, Phys. Rev. B 48 (1993) 2074.
[29] J.F. Moulder, W.F. Stickle, P.E. Sobol, K.D. Bomben, Handbook of X-ray Photoelectron Spectroscopy, Physical Electronics, Inc., Eden Prairie, MN, 1995.
[30] B. Erdem, R.A. Hunsicker, G.W. Simmons, E.D. Sudol, V.L. Dimonie, M.S. El-Aasser, Langmuir 17 (2001) 2664–2669.
[31] W.E. Kaden, T. Wu, W.A. Kunkel, S.L. Anderson, Science 326 (2009) 826–830.
[32] U. Diebold, T.E. Madey, Surf. Sci. Spectra 4 (1996) 227–231.
[33] R.L. Kurtz, Surf. Sci. Spectra 5 (1998) 182–185.
[34] J. Ji, G. Zhang, H. Chen, Y. Li, G. Zhang, F. Zhang, Z. Fan, J. Mater. Chem. 21 (2011) 14498–14501.
[35] Y. S. Yang, S. Kim, K.-J. Kim Park, Chem. Asian J. 6 (2011) 2362–2367.
[36] V.I. Iliev, A.I. Ileva, L.D. Dimitrov, Appl. Catal., A: General 126 (1995) 333–340.

Update

Applied Catalysis B: Environmental
Volume 185, Issue , 15 May 2016, Page 379

DOI: https://doi.org/10.1016/j.apcatb.2015.12.047

Applied Catalysis B: Environmental 185 (2016) 379

Contents lists available at ScienceDirect

Applied Catalysis B: Environmental

journal homepage: www.elsevier.com/locate/apcatb

Erratum

Erratum to "Photocatalytic oxidation activities of TiO_2 nanorod arrays: A surface spectroscopic analysis" [Appl. Catal. B: Environ. 180 (2015) 480–486]

Yun Jeong Hwang[a], Sena Yang[b], Eun Hee Jeon[b], Hyun Woo Nho[c], Ki-Jeong Kim[d], Tae Hyun Yoon[c], Hangil Lee[e,*]

[a] Clean Energy Research Center, Korea Institute of Science and Technology, Seoul 136-791, Republic of Korea
[b] Molecular-Level Interface Research Center, Department of Chemistry, KAIST, 305-701, Republic of Korea
[c] Department of Chemistry, Hanyang University, 222 Wangsimniro, Seoul 133-791, Republic of Korea
[d] Beamline Research Division, Pohang Accelerator Laboratory (PAL), Pohang 790-784,Republic of Korea
[e] Department of Chemistry, Sookmyung Women's University, Seoul 140-742, Republic of Korea

The publisher regrets to inform that Fig. 7 was published wrongly in the original article. Please find the correct version of Fig. 7. Publisher would like to apologize for the inconvenience caused.

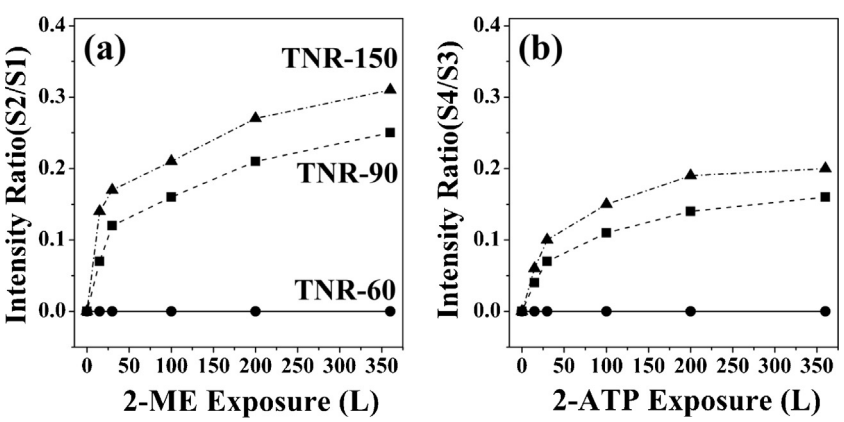

Fig. 7. The ratios of the intensities of (a) S2 and S1 and (b) S4 and S3 adsorbed on the three distinct TiO_2 NR samples as functions of molecular exposure under 365 nm UV light.

DOI of original article: http://dx.doi.org/10.1016/j.apcatb.2015.07.004.
* Corresponding author. Fax: +82 2 2077 7321.
E-mail address: easyscan@sookmyung.ac.kr (H. Lee).

http://dx.doi.org/10.1016/j.apcatb.2015.12.047